Energy 248 (2022) 123537

Contents lists available at ScienceDirect

Energy

journal homepage: www.elsevier.com/locate/energy

Adaptive online capacity prediction based on transfer learning for fast charging lithium-ion batteries

Zhang Chen [a], Wenjing Shen [a], Liqun Chen [b, *], Shuqiang Wang [c]

[a] Sino-German College of Intelligent Manufacturing, Shenzhen Technology University, Shenzhen, 518118, China
[b] College of Urban Transportation and Logistics, Shenzhen Technology University, Shenzhen, 518118, China
[c] Shenzhen Institutes of Advanced Technology, Chinese Academy of Sciences, Shenzhen, 518055, China

ARTICLE INFO

Article history:
Received 16 November 2021
Received in revised form
16 February 2022
Accepted 18 February 2022
Available online 28 February 2022

Keywords:
Lithium-ion battery
Capacity prediction
Fast charging
Integrated feature
Adaptivity
Transfer learning

ABSTRACT

The aging of the battery is complicated and depends on both internal and external factors. Fast charging will amplify the cell-to-cell differences and make battery capacity prediction more challenging. In this paper, a long short-term memory network-based transfer learning model is proposed for adaptive online capacity prediction under fast charging. First, a novel voltage feature of charging to 80% state of charge in about 10 min is introduced. A sliding window is designed to integrate the voltage feature and the cycle number. The feature is highly practical and can be easily measured in all fast charging conditions. Second, to deal with the cell-to-cell differences and improve the model adaptivity, a cross-validation method with both high- and low-similarity tasks is performed to derive optimal hyperparameters. Then, the offline model can be trained using the existing complete battery lifespan data. Third, with the arrival of new battery data, the model can be finetuned at the full connected layer. The well-adjusted model can be applied for online capacity prediction. The other four features are compared to prove the superiority of the proposed feature. Six experiments with different fast charging conditions are carried out to verify the effectiveness and adaptability of the proposed method.

1. Introduction

Lithium-ion batteries (LIBs) have the advantages of high energy density, long cycle life, and low memory effect. They are currently the first choice for electric vehicles (EVs). To ensure driving safety, LIB's state of health (SOH) needs to be carefully monitored in real-time with high accuracy and adaptability.

Capacity and internal resistance are common health indicators (HIs) to quantify battery degradation [1]. However, due to the incomplete discharge and inconsistency of LIBs used in groups, it is difficult to directly measure these HIs online [2,3]. The up-to-date degradation modeling consists of two key steps. First, features are extracted from battery voltage, current, and temperature data [4]. Then, the mapping relationship between features and HIs is established to reflect the SOH of LIB.

In practical applications, the aging rate of the battery varies significantly due to complex internal mechanisms (including ion diffusion, charge transfer process, and ohmic effect) and external factors (such as temperature, charge and discharge rate, and depth of discharge) [5]. In addition, some improper operating conditions, such as high current or extreme temperature, will amplify the impact of battery manufacturing defects on the degradation behavior [6,7]. The resulting cell-to-cell differences make accurate and adaptive SOH prediction a challenging task.

LIBs SOH prediction methods can be classified into two categories: model-based methods and data-driven methods. Representative model-based methods include electrochemical models, equivalent circuit models (ECMs), and empirical models. Based on the first principal knowledge, electrochemical models can describe internal processes of LIBs, such as the loss of lithium inventory and active materials [8], to achieve accurate SOH prediction. However, they also require high computational complexity by solving partial differential equations [9]. ECMs use a set of electrical components to simulate the dynamic response and degradation behavior of LIBs and the electrochemical impedance spectroscopy (EIS)/open circuit voltage (OCV) data can be used to identify ECM parameters [10]. Typical ECMs include Rint model [11], first-order RC model [12], and Thevenin model [13]. Besides, a fractional-order ECM model [14] is proposed to improve accuracy and robustness, and the

* Corresponding author.
E-mail address: chenliqun@sztu.edu.cn (L. Chen).

https://doi.org/10.1016/j.energy.2022.123537
0360-5442/

optimization and filtering algorithms are used for parameter updates. Furthermore, considering the underlying coupling states at different time scales, a novel hierarchical co-estimation framework [15] is designed to provide more accurate and reliable estimates at a limited computational cost. However, in real-time applications, EIS/OCV testing is very time-consuming and the equipment may not be useable [1]. Empirical models establish the correlation of LIBs data and incorporate common features of battery degradation behavior [1]. They can be easily implemented using regression models or empirical formulas to fit and forecast the degradation state. However, the identified parameters are susceptible to noise, which makes the robustness of this method low [4].

In view of the above considerations, data-driven methods are widely studied for SOH prediction due to their nonlinear mapping capability and flexibility [9,16]. Typical methods include support vector machine (SVM), relevance vector machine (RVM), Gaussian process regression (GPR), and artificial neural network (ANN). In Refs. [17–19], SVM-based models are established when there are enough training samples. However, they are sensitive to missing data. To deal with the data uncertainty, RVM- [20,21] and GPR-based models [22,23] are developed based on the Bayesian framework. Although the modeling performance can be slightly improved, these methods have high requirements for time and memory. In addition, the kernels need to be carefully selected [16].

Compared to non-parametric algorithms, ANN can achieve higher robustness when the sample data is sufficient. Currently, recurrent neural networks (RNNs) [24,25] have been introduced for SOH estimation, in which long short-term memory (LSTM) is reported as a powerful RNN to learn long-term dependencies [26]. You et al. [27] used LSTM to construct a SOH prediction model corresponding to various driving modes in the dynamic cycle. Li et al. [28] created an offline capacity estimation model suitable for EVs in actual operation. This model is valid in case of noise interference and missing data. Then, they [29] proposed an online prognostics framework based on LSTM, which trains the model in the cloud and provides it to the battery management systems (BMSs) of EVs. Zhang et al. [30] combined LSTM with Monte Carlo simulation to generate a probabilistic remaining useful life (RUL) prediction model. Its long-term learning performance is better than the SVM model and the simple RNN model. Cheng et al. [31] and Liu et al. [32] predicted SOH and RUL based on LSTM. LSTM-based methods can achieve promising accuracy and robustness. However, the computational cost is still a bottleneck for large-scale applications. It is reflected in two aspects:1) the structure of the LSTM needs to be implemented through a lot of trials [28,29,31]; 2) the online prediction model needs to be continuously retrained with the arrival of new data [27,30,32]. Moreover, the well-trained models can only be used for the same batch of batteries, resulting in low adaptability.

To reduce the burden of online computing, few studies have introduced transfer learning into LSTM-based models. Che et al. [33] designed a transfer learning model using gated LSTM. A self-correction strategy is proposed to retrain the regression model to achieve online capacity prediction. However, this method is only suitable for LIBs with highly similar degradation patterns. Tan et al. [34] proposed a LIBs SOH prediction model combined with two fully connected (FC) layers. During transfer learning, the LSTM is frozen to capture similar properties of long-term dependencies, and the FC layers are adjustable to learn the private properties of different LIBs. Although this method can be used for LIBs with highly different degradation patterns (DPs), the model adaptivity still needs to be improved. First, the representative task needs to be carefully selected for model training. Second, the model structure and hyperparameters need to be changed according to different tasks. Further, Deng et al. [35] classified cells into three DPs (namely, short, medium, and long lifetime), and trained the corresponding model with the reference cell data for each DP. They realized DP recognition and transfer learning based on early aging data, which effectively solved the DP difference caused by operating conditions and improved the SOH estimation accuracy. However, DP recognition may increase complexity, and wrong DP recognition may threaten the robustness of predictive models. Tian et al. [36] innovatively developed a transfer learning model to estimate the entire charging curve, thereby deriving key battery states, such as capacity and energy. The model can be used for different batteries under different working conditions. Their research is exciting, but it only applies to constant current (CC) charging data, not fast charging.

In addition to the model structure, features will also play a decisive role and significantly affect prediction performance. Features can be extracted from both the charging and discharging phases. The features extracted from the discharging phase can better reflect the battery degradation during cycling. In Refs. [37,38], the discharge time or RC model parameter features are extracted from the random variable current (VC) discharge data. In this method, a complete discharge process is required, and the extracted features need to be fitted or filtered to reduce data fluctuations. The features can also be obtained from current and voltage curves using incremental capacity (IC) and differential voltage (DV) analysis [35,39]. These features can detect subtle changes in electrochemical processes caused by the capacity loss [4]. However, the capacity measurement requirements and heavy calculational burden make them not appliable to online prediction. In Ref. [23], the voltage-temperature (VT) features, including the intercept b, the slope w, and the thermal-dependent feature T, are extracted to improve the SOH prognostics of LIBs. However, continuous CC discharge is required, which is inconsistent with the actual working conditions.

The features extracted in the charging phase are more stable because of the fixed charging strategy. They can be extracted directly from voltage, current, and temperature curves [4]. Tan et al. [34] treated interval points and integral of voltage versus time as features. Wang et al. [40] introduced a time constant from the charging current curve to indicate the aging state of the battery. Fei et al. [41] selected the minimum and average temperature to reflect battery life. The disadvantage of the above features is that a long curve interval or even a complete charging curve is required. Besides, the temperature-based features are susceptible to environmental interference. The IC-based [42,43] and DV-based [44] features can also be derived from the charging process. However, these features are extracted from CC-constant voltage (CC-CV) charging conditions and are unsuitable for fast charging strategies.

In Refs. [22,45], the cycle number is considered a feature. Different from the above features, the mapping relationship between cycle number and capacity can be established directly, and no charging/discharging curve is required. Moreover, the cycle number is considered to be a common parameter for developing capacity degradation model [45]. Due to changes in cycling operating conditions and lack of first-principles information, the method is simple but less accurate.

In summary, there are two challenging issues in LIB SOH prediction:

(1) Poor practicability of extracted features: the features extracted in the discharging phase do not match the actual working conditions, and the features extracted in the charging phase are not appliable to fast charging strategies.
(2) Low adaptability of the prediction model: the cell-to-cell differences pose a threat to the generalization ability of the model.

Motivated by these considerations, this paper proposes a LSTM-FC network-based transfer learning model for adaptive online battery capacity prediction. To improve the practicability, a novel voltage feature of charging to 80% state of charge (SOC) and resting for 10 s is introduced to indicate the SOH of LIB. The Pearson correlation analysis is conducted to validate the effectiveness of the feature. To solve the issue of low adaptability, a two-stage model is developed. In the offline stage, hyperparameters are first tuned using high- and low-similarity tasks with different degradation patterns. The optimal hyperparameters can be obtained by finding the common area through multi-task cross-validation. Then, the existing battery life data can be used for offline model training. In the online prediction stage, the LSTM is frozen to capture shared properties, and the FC layer is finetuned based on the new battery data to adapt to cell-to-cell differences. Six experiments with different fast charging conditions, plus four other features, are carried out to validate the effectiveness and adaptivity of the proposed method.

The contributions of this paper are:

(1) A novel health feature, the terminal voltage when the battery is charged to 80% SOC for about 10 min, is introduced to indicate the LIB capacity. It has high practicability and can be used for various fast charging conditions.
(2) A highly adaptable transfer learning model based on the LSTM-FC network is proposed. By using the high- and low-similarity tasks optimization method, it can be used to predict the battery capacity with different degradation patterns.
(3) Experiments on two CC fast charging conditions, two VC fast charging conditions, and two cross fast charging conditions have been conducted to verify the superiority of the proposed method.

The rest of this paper is organized as follows: Section 2 introduces the degradation feature extraction. Section 3 describes the methodologies. Results and analysis are given in Section 4, and conclusions are presented in Section 5.

2. Degradation feature extraction

2.1. Experimental data

The battery dataset used in this work comes from accelerated aging experiments conducted by the Massachusetts Institute of Technology and Stanford University [39]. The experiments were originally designed to explore the battery capacity degradation due to complex aging mechanisms and manufacturing variability under different fast charging conditions. They aim to achieve early cycle life prediction and lifespan classification. This dataset consists of 124 LFP batteries produced by A123 Systems. The key technical indicators of these batteries are listed in Table 1. The ambient temperature is set as 30 °C using a chamber. All batteries are cycled under different fast charging conditions but identical discharging conditions (4C–2.0 V, where 1C is 1.1 A).

Table 1
Technical indicators of experimental LIBs.

Manufacturer	A123 Systems
Type	APR 18650M1A
Cathode/Anode	$LiFePO_4$/Graphite
Rated capacity/Rated voltage	1.1 Ah/3.3 V
Cut-off voltages	3.6 V, 2 V
Environmental temperature	30 °C
Discharging current	4C

Under fast charging conditions, batteries are first charged to 80% SOC through two-step high CC rates. The average fast charging rates range from 3.6C to 6C, and the fast charging time is near 10 min. After resting for 10 s, the batteries are charged to full SOC through the CC-CV strategy (1C–3.6 V).

The capacity degradation curves of these batteries are shown in Fig. 1(a). When cycling to 80% of the nominal capacity, these batteries are considered to have reached the end-of-life (EOL) threshold. As charging conditions change, a wide range of battery life degradation data can be captured. The cycle number ranges from approximately 150 to 2,300. Compared with other publicly available datasets, such as those provided in Ref. [46], where the maximum difference of all 48 cells is only about 200 cycles, the dataset chosen here is more challenging.

The variability of capacity degradation in this dataset includes the nonlinear difference of the aging rate at each stage and the cell-to-cell differences. Here, the data with unreasonable charging conditions that lead to premature battery failure are discarded, and the data with medium and long battery life are chosen. According to the charging strategy, the remaining batteries can be divided into conditions 1–5 as shown in Fig. 1(b)–(f). For example, in condition 5, the batteries are firstly charged to 19% SOC using 5.6C, and then charged to 80% SOC using 4.6C. It can be seen from Fig. 1(b)–(f) that under the same charging conditions, the batteries still exhibit significant degradation variability due to the high current rate amplifying the manufacturing defects [7,16,47].

2.2. Voltage feature extraction

In this paper, the feature is extracted from the charging phase. It is defined as the voltage at which the battery is charged to 80% SOC and rested for 10 s. Define $V_{80\%}$ as the corresponding extracted voltage feature. Since the proposed feature is a point, it has high practicability and can be easily measured in various fast charging strategies.

Fig. 2(a) denotes the data of all batteries in five fast charging conditions. Fig. 2(b) depicts the current and voltage curves from representative No.85 battery in condition 3 during charging and discharging in the 1st and 1008th cycles. The red dots are the corresponding voltage features. Fig. 2(c) is the graphical representation of 1008 features extracted from the lifespan of this battery. The $V_{80\%}$ feature curves extracted from all batteries in conditions 1–5 are shown in Fig. 2(d). As the cycle number increases, $V_{80\%}$ rises monotonically, and its rising rate is similar to the decreasing rate of capacity. When the failure threshold is reached, the $V_{80\%}$ feature values of all batteries are close to the upper cut-off voltage and are within the statistical $\pm 3\sigma$ confidence interval. The $\pm 3\sigma$ confidence interval is less than 0.01 V, which well reflects the degradation process.

2.3. Pearson correlation analysis

To verify the effectiveness of the extracted features, the Pearson correlation coefficient (PCC) [23,25,39] is used as the evaluation criteria to quantify the relationship between capacity and features. The closer the absolute PCC is to 1, the better the correlation is.

The PCC is calculated as:

$$r = \frac{\sum_{j=1}^{N}(F_j - \overline{F})(Q_j - \overline{Q})}{\sqrt{\sum_{j=1}^{N}(F_j - \overline{F})^2}\sqrt{\sum_{j=1}^{N}(Q - \overline{Q})^2}} \quad (1)$$

where F and Q represent the extracted feature and target capacity, the subscript j is the j_{th} cycle, and the upper line stands for the

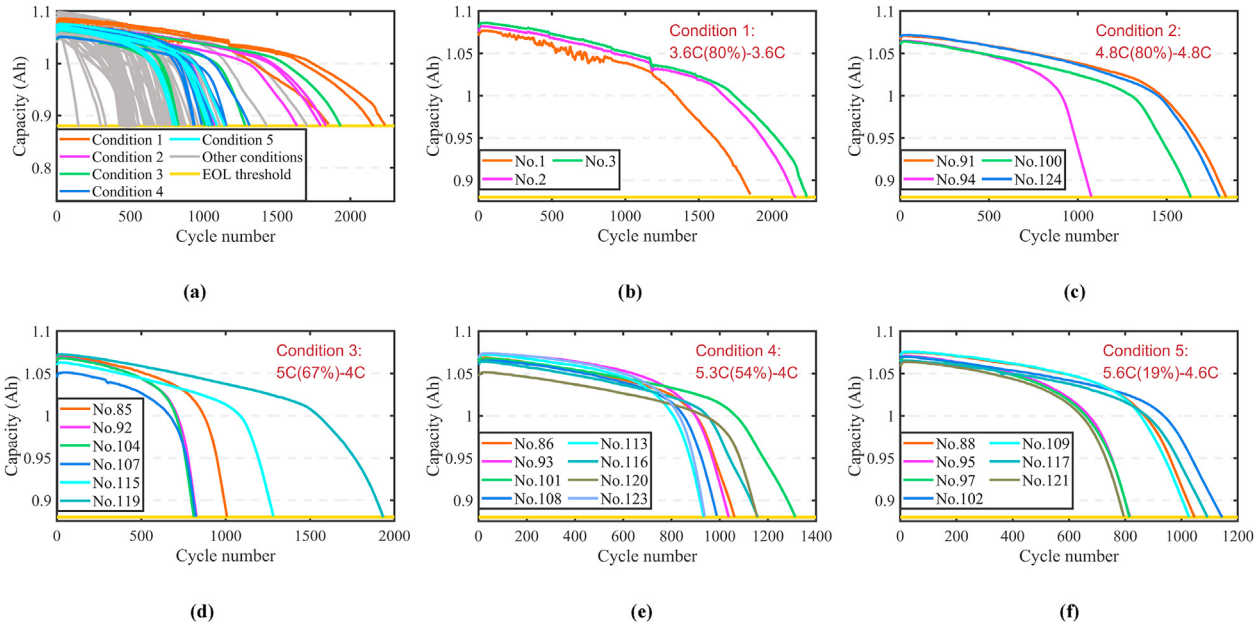

Fig. 1. Capacity degradation curves of LIB dataset under different fast charging conditions.

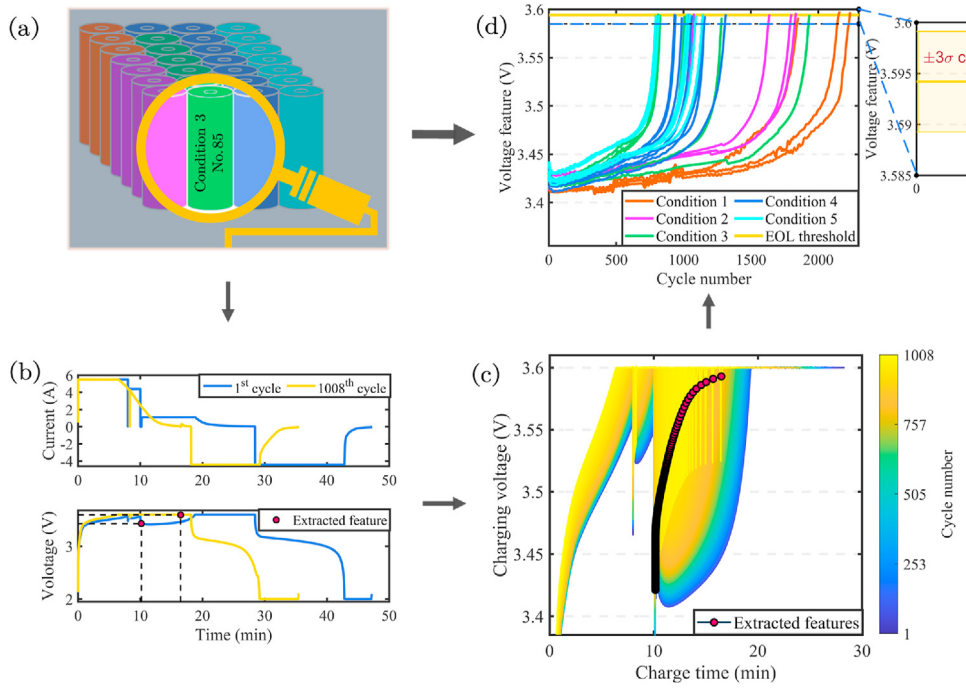

Fig. 2. **(a)** 28 batteries in fast charging conditions 1–5; **(b)** Current and voltage curves at the 1st and 1008th charging and discharging of No.85 battery in condition 3; **(c)** Extracted $V_{80\%}$ features from 1008 cycles of this battery; **(d)** $V_{80\%}$ feature curves extracted from all 28 batteries.

average mean operation.

Five representative batteries are chosen from charging conditions 1–5. The calculated absolute PCCs are summarized in Table 2. The lowest PCC is 0.9657, which is very close to 1, from the No. 1 battery in condition 1. It proves that there is a good linear correlation between the proposed feature and the capacity. Another four features, the intercept feature *b*, the slope feature *w*, the thermal-dependent feature *T* in Ref. [23], and the cycle number feature Cn in Refs. [22,45] are added for comparison. As shown in Table 2, the maximum PCC of *T* [23] is less than 0.6, and the minimum is less

Table 2
Absolute PCCs between features and capacity.

	Condition 1	Condition 2	Condition 3	Condition 4	Condition 5
	No.1	No.91	No.85	No.86	No.88
$V_{80\%}$	0.9657	0.9714	0.9844	0.9857	0.9731
b	0.9370	0.9811	0.9929	0.9934	0.9876
w	0.9215	0.9464	0.9707	0.9470	0.9686
T	0.0903	0.4506	0.2174	0.5972	0.0609
Cn	0.9270	0.8866	0.8333	0.8369	0.8532

than 0.1. The PCCs of Cn are between 0.83 and 0.93. It indicates that there is also a good correlation between the cycle number Cn and the capacity. The PCCs of the intercept feature b and the slope feature w are more than 0.92, which are comparable to the proposed feature $V_{80\%}$.

2.4. Integrated feature

This paper proposes a novel feature that integrates the voltage feature $V_{80\%}$ with the cycle number Cn to further improve the mapping ability. The voltage feature $V_{80\%}$ reflects the private attributes closely related to the battery degradation process. The cycle number Cn reflects the common characteristics of cycle aging of all batteries [16,45]. It provides the model with general knowledge of battery degradation. The combination of private and common attributes can better reflect the battery's aging, thereby providing more accurate capacity prediction performance.

A sliding window (SW) [48] is introduced to deal with the strong nonlinearity in capacity degradation, as shown in Fig. 3. By an SW, the most recent voltage feature, which can truly reflect the real-time intrinsic nature of the degradation process, will be utilized for modeling. As time updates, the SW Φ_t moves forward, and the integrated feature can be expressed as:

$$\Phi_t = [\, v_{t-l} \quad v_{t-l+1} \quad \cdots \quad v_t \quad Cn_t \,] \tag{2}$$

where $l+1$ is the SW size, v_t and Cn_t denote the $V_{80\%}$ feature and the current cycle number at time t, respectively.

3. Methodologies

3.1. Model framework

In this paper, a LSTM-FC network-based transfer learning model is proposed for adaptive online capacity prediction. An overview of the framework is shown in Fig. 4. It consists of two parts, namely offline model development and online application.

The offline model development includes two procedures. In procedure 1, hyperparameters are tuned using high- and low-similarity tasks with different degradation patterns in condition 5. The optimal hyperparameters are obtained by finding the common area through multi-task cross-validation optimization. In procedure 2, the complete life cycle data from partial batteries in conditions 1–4 are used for offline model training. After good training, the offline model is sent to the online applications. In the online application, the LSTM is frozen to keep sharsed properties, and the FC layer is fine tuned to adapt to cell-to-cell differences when the new battery data is available.

To quantitatively evaluate the model performance, the root mean square error (RMSE) and the mean absolute percentage error (MAPE) are used:

$$RMSE = \sqrt{\frac{1}{n}\sum_{t=1}^{n}(Q_t - \widehat{Q}_t)^2} \tag{3}$$

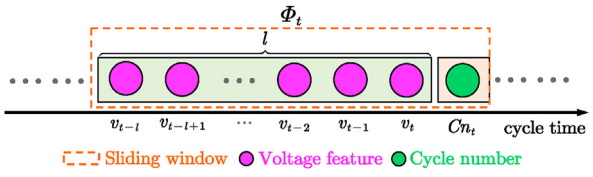

Fig. 3. Integrated feature through SW technology.

$$MAPE = \frac{1}{n}\sum_{t=1}^{n}\left|\frac{\widehat{Q}_t - Q_t}{Q_t}\right| \times 100\% \tag{4}$$

where n is the total size for online prediction.

3.2. LSTM-FC network

The LSTM network is used to construct a transfer learning model for capacity prediction. LSTM is originally proposed by Hochreiter and Schmidhuber [26]. It is popular and has been widely used to model complex nonlinear systems. LSTM can better learn long-term dependent information in battery aging data, and provide more powerful nonlinear mapping capabilities than simple regression networks or other machine learning methods.

The proposed LSTM-FC network architecture consists of an input layer, a LSTM layer, a FC layer, and an output layer. The LSTM layer is composed of a series of recurrent neurons, and each cell has three gates to decide whether to forget or write input information. The cell operation [28] is described as follows.

Forget gate: A forget gate f_t is set to determine what information should be discarded from the current cell.

$$f_t = \sigma\left(w_f \cdot [h_{t-1}, x_t] + b_f\right) \tag{5}$$

where σ is the sigmoid activation function, the indications of w and b are similar in this section, e.g., w_f and b_f represent the weighted matrix and bias of f gate, respectively, x_t is the input, h_{t-1} is hidden output state, and the subscript t denotes the current time step.

Input gate: An input gate i_t is set to determine what new information should be updated into the current cell.

$$i_t = \sigma(w_i \cdot [h_{t-1}, x_t] + b_i) \tag{6}$$

$$\tilde{C}_t = \tanh(w_C \cdot [h_{t-1}, x_t] + b_C) \tag{7}$$

$$C_t = f_t * C_{t-1} + i_t * \tilde{C}_t \tag{8}$$

where tanh is the hyperbolic tangent activation function, $\tilde{C}_t$ is the candidate state, C_t is the current cell internal state, and the $(*)$ is the element-wise multiplication operator.

Output gate: The output gate generates the current output state vector o_t. The o_t is multiplied by the new cell state C_t through a tanh layer (to push the values to be between -1 and 1) to obtain the new output state h_t.

$$o_t = \sigma(w_o \cdot [h_{t-1}, x_t] + b_C) \tag{9}$$

$$h_t = o_t * \tanh(C_t) \tag{10}$$

To deal with cell-to-cell differences, a FC layer is designed for the transfer learning model to learn the specific properties from the predicted battery. The final predicted capacity $\widehat{Q}_t$ at step t can be calculated as:

$$\widehat{Q}_t = w_Q \cdot (w_h \cdot h_t + b_h) + b_Q \tag{11}$$

During the transfer learning, the front LSTM layer is frozen, and the FC layer is fine-tuned based on the new battery data. Since the FC layer is a linear model related to input h_t and output $\widehat{Q}_t$, it has low computational complexity and is suitable for online prediction.

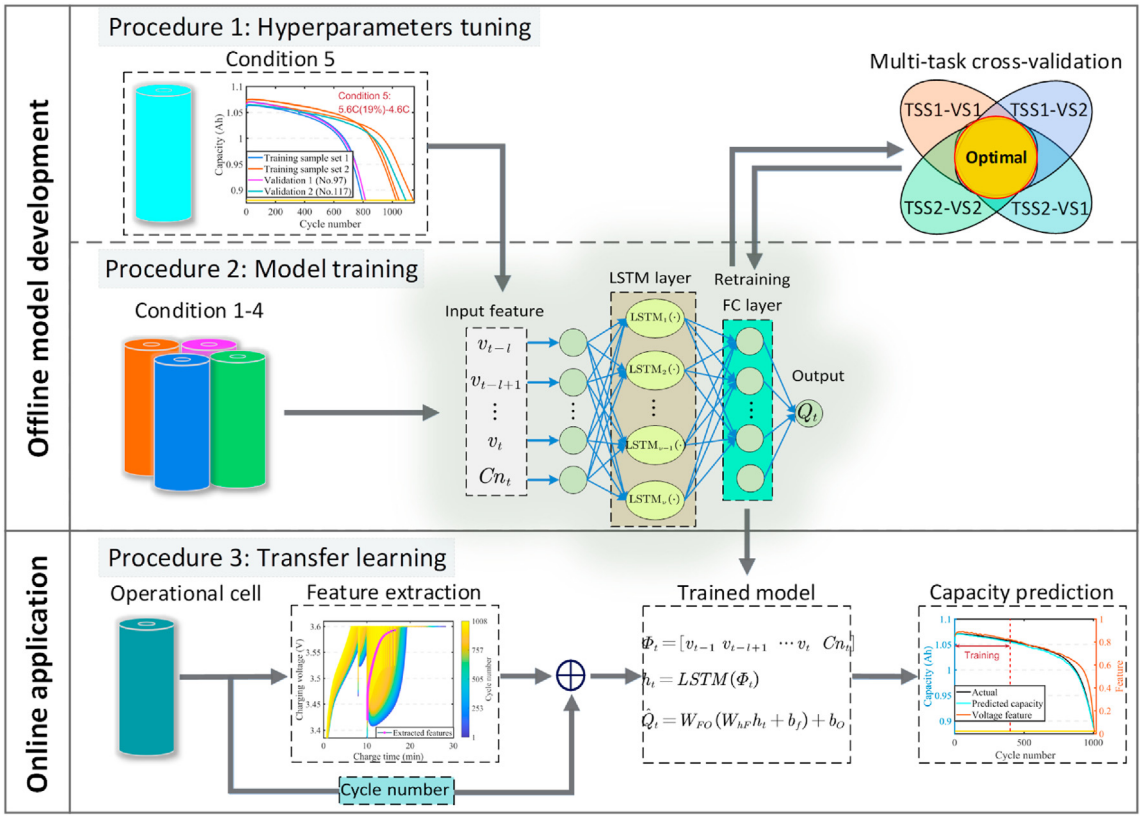

Fig. 4. Flowchart of the proposed adaptive online capacity prediction method for LIBs based on transfer learning.

3.3. Hyperparameters tuning

The existing transfer learning-based models mainly consider similar tasks [33] or rely heavily on prior knowledge [34,36]. Therefore, its adaptivity and generalization ability are low.

To deal with cell-to-cell differences, a multi-task cross-validation method is used for hyperparameter tuning. The condition 5 dataset is used here. As shown in Fig. 5(a), the seven LIBs are divided into four parts, namely, training sample set 1 (TSS1), training sample set 2 (TSS2), validation sample 1 (VS1), and validation sample 2 (VS2). TSS1 consists of No. 95 and No. 121 batteries, TSS2 includes No.88, No. 102, and No. 109 batteries, VS1 has No.97 battery, and VS2 has No. 117 battery.

Four tasks are formed according to the similarity between TSS and VS. High similarity tasks include TSS1-VS1 and TSS2-VS2. Low similarity tasks consist of TSS1-VS2 and TSS2-VS1. In each task, the model is first trained using TSS, and then finetuned using VS. The optimizer Adam [49] is used to accelerate training. Regularization is achieved by combining dropout [50] with L2 Regularization (L2R) [30]. It can reduce the complexity and instability of the model, thereby reducing the chance of overfitting.

The crucial hyperparameters, including the number of LSTM neuron and FC unit, SW size, learning rate, and fine tune epoch, are sequentially optimized by grid search under the condition of fixing other hyperparameters. The LSTM-FC model is first trained using TSS, and then finetuned using the first 400 cycles of data in VS.

Take the SW size as an example, the is sampled from {1, 2, 3, …, 30}, as shown in Fig. 5(b). For high similarity tasks TSS1-VS1 and TSS2-VS2, the prediction RMSE climbs slowly with the rise of SW size. It is reasonable that the large size of $V_{80\%}$ will make the model

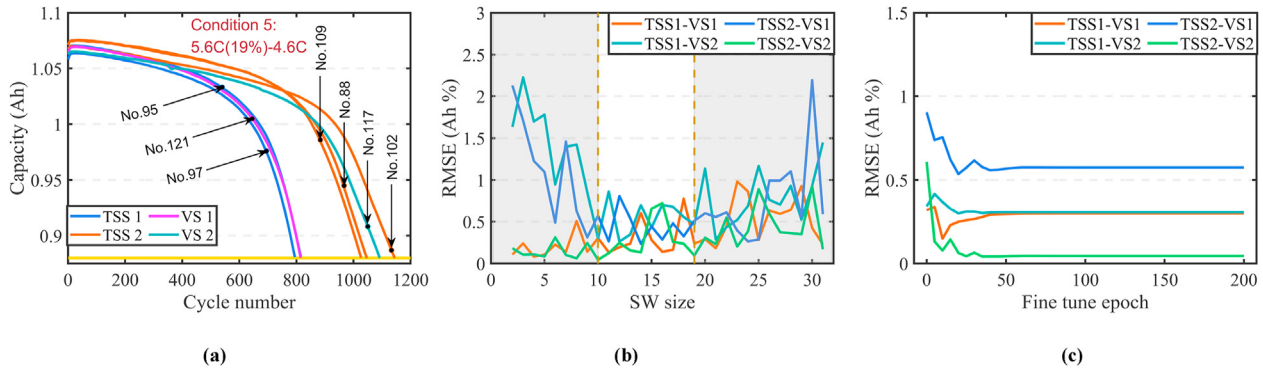

Fig. 5. Multi-task cross-validation. **(a)** Dataset for hyperparameters tuning; **(b)** SW size validation (The white area is the optimal interval); **(c)** Fine tune epoch validation.

learn too much early degradation information, thereby increasing the capacity prediction error for the mid-and late-stages of the nonlinear aging LIB. It is academically called “negative transfer” [51]. As a result, a small SW size is required for high similarity tasks. For low similarity tasks TSS1-VS2 and TSS2-VS1, the prediction RMSE first decreases and then slightly increases as the size of $V_{80\%}$ feature increases. Then, a larger SW size is needed. Considering all these tasks comprehensively, the optimal SW size interval is [10,19], where the prediction RMSE is stable and low. In this paper, the final SW size is set to 10, that is, $l = 9$.

As shown in Fig. 5(c), the fine tune epoch is tested from {0, 10, 20, …, 200}. When fine tune epoch exceeds 50, all curves reach a stable level. As a result, the fine tune epoch is set to 50. Similarly, as Fig. 4 shows, by finding the common area of tuned hyperparameters deriving from four tasks, the optimal hyperparameters can be obtained. The optimal hyperparameters are summarized in Table 3.

3.4. Offline model training

The four battery datasets of conditions 1–4 are used for offline model training. Before training, the feature and capacity labels need to be normalized for better model performance:

$$v_t = \frac{V_{80\%}(t) - 3.595}{3.4 - 3.595} \tag{12}$$

$$Cn_t = \frac{t}{\overline{EOL}_{tr}} \tag{13}$$

$$Q_t = \frac{Q_r(t) - 0.88}{1.1 - 0.88} \tag{14}$$

where v_t, Cn_t, and Q_t are the normalized values of the $V_{80\%}$ feature, the Cn, and the raw capacity Q_r respectively in the tth cycle; $\overline{EOL}_{tr}$ is the mean EOL of training samples; 3.595 and 3.4 in (12) represent the upper and lower voltage limits of the curves in Fig. 2(d); 1.1 and 0.88 in (14) indicate the normal capacity and EOL threshold of the LIBs.

3.5. Transfer learning-based online prediction

After the well-trained model achieved by the above steps is sent to the BMS, the transfer learning method can be used for online capacity prediction. To deal with the cell-to-cell differences, the battery data in the early period is employed to retrain the FC layer while keeping the front LSTM layer unchanged. In this paper, all cases use the first 400 cycles of data from the testing batteries for finetuning. As shown in (11), only four matrices w_Q, w_h, b_h, and b_Q in the FC layer need to be updated. Therefore, this method has low computational complexity and is suitable for online prediction.

Table 3
Optimal hyperparameter settings of LSTM-FC network.

	Fixed		Optimized	
Stage	Parameter	Value	Parameter	Value
Training	Epoch	500	LSTM neuron	100
	Batch size	128	FC unit	15
	L2R	0.0002	SW size	10
	Dropout	10%	Learning rate	0.05
Fine tuning	Batch size	16	Learning rate	0.005
	L2R	0.01	Fine tune epoch	50
	Dropout	10%		

4. Results and analysis

First, the effectiveness of the model framework is verified by comparing with Ref. [23]. Second, the practicability of the novel feature is analyzed by comparing with the other four features. Third, the adaptability of the proposed method is validated by six experiments under different fast charging conditions.

4.1. Model framework comparison

A comprehensive comparison is made with Ref. [23] to prove the effectiveness of the proposed model framework. In Ref. [23], the No.91 and No.100 batteries in Condition 2 are used for training, and the No.124 battery is used for testing. The VT features are extracted, and the GPR is used to build a capacity prediction model. The prediction RMSE in Ref. [23] is 0.6900%. Keeping the same experimental dataset and design, the prediction RMSE of the proposed method is 0.2465%, which is much lower than that in Ref. [23]. To exclude the effect of the feature, the VT features in Ref. [23] and the LSTM-FC model framework proposed in this paper are added for model performance comparison. Its prediction RMSE is 0.5472%, which is 20.7% lower than that in Ref. [23]. It can be considered a big improvement. Since the experimental design and dataset are the same, it proves that the proposed LSTM–FC–based transfer learning model is feasible and effective.

4.2. Feature comparison

To further verify the practicability and superiority of the proposed feature, another four different features, including $V_{80\%}$, Cn [22,45], VT [23], and VT + Cn, are added for model performance comparison. Fig. 6–8 show the predicted capacity and error of all six different fast charging cases. The numerical results are summarized in Table 4.

For the single $V_{80\%}$ feature, the prediction RMSEs and MAPEs are lower than those of the VT and Cn features in all six cases. It shows that the $V_{80\%}$ feature can better reflect the aging behavior of LIBs, and is more conducive to establishing a mapping relationship with capacity. Especially in the late stage of degradation, as shown in Fig. 6(a) and (d), Fig. 7(a) and (d), and Fig. 8(a) and (d), the capacity curve predicted by the $V_{80\%}$ feature overlaps well with the actual curve. It is reasonable. As mentioned earlier in Fig. 2(d), the increase rate of the $V_{80\%}$ feature is similar to the decrease rate of the capacity. When the capacity reaches the EOL threshold, all the $V_{80\%}$ feature curves rise to a position close to the upper cut-off voltage.

For the integrated $V_{80\%}$ + Cn feature, its capacity prediction RMSE and MAPE are the lowest in all six cases compared to the other four features. Compared with the $V_{80\%}$ feature, it proves the beneficial effect of adding the cycle number Cn. The Cn feature reflects the common characteristics of cycle aging [16,45]. Therefore, the integrated feature $V_{80\%}$ + Cn makes use of not an only private attribute but also common information of all batteries, thereby greatly improving the model adaptability. It can be seen in Figs. 6–8 (b) and (e) that the addition of the cycle number Cn makes the model performance more stable, thereby further reducing the prediction error. Compared with the VT + Cn feature, it further verifies the practicability of the proposed $V_{80\%}$ feature.

4.3. Model adaptability verification

To verify the adaptivity of the proposed method, six comparative cases are conducted under different fast charging conditions, as shown in Table 4.

Cases 1 and 2 are CC fast charging conditions. Take case 1 as an example, the training samples are No. 1 and No.3 batteries and the

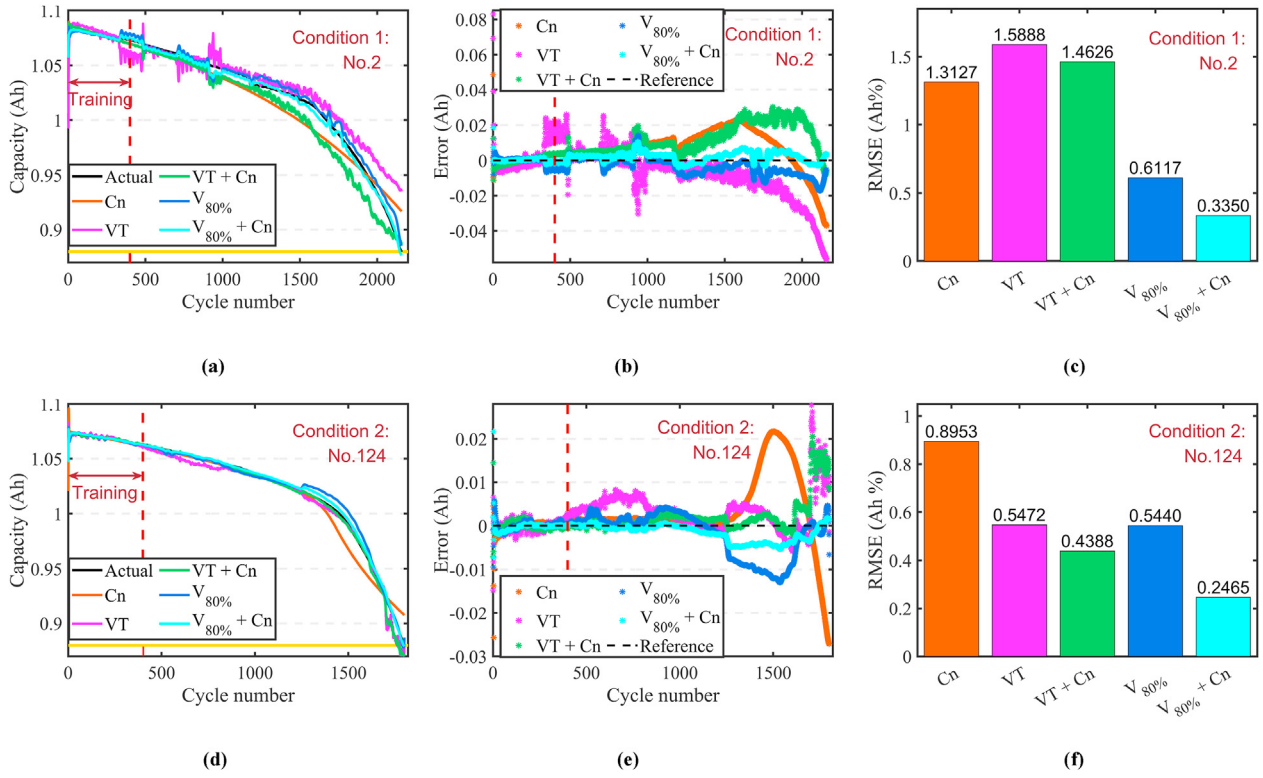

Fig. 6. Capacity prediction performance for CC fast charging conditions. **(a)**, **(b)** and **(c):** Case 1; **(d)**, **(e)** and **(f):** Case 2.

Table 4
Capacity prediction performance comparison of five features with six fast charging conditions.

Case No.	Training samples	Testing cell	Criteria (%)	$V_{80\%}$ + Cn	$V_{80\%}$	VT + Cn	VT	Cn
1	Condition 1	Condition 1	RMSE	**0.3350**	0.6117	1.4626	1.5888	1.3127
	No. 1, No.3	No.2	MAPE	**0.2820**	0.4902	1.2247	1.1553	1.1141
2	Condition 2	Condition 2	RMSE	**0.2417**	0.5697	0.5844	0.7975	0.8953
	No.91, No.100	No.124	MAPE	**0.1756**	0.4514	0.4466	0.5352	0.5622
3	Condition 3	Condition 3	RMSE	**0.3972**	1.7533	1.0937	1.9386	5.9599
	No.85, No.107, No.115	No.119	MAPE	**0.3190**	1.4959	0.8630	1.7264	5.0013
4	Condition 4	Condition 4	RMSE	**0.3637**	0.8966	0.8010	1.0165	1.3643
	No.93, No.113, No.120	No.116	MAPE	**0.3320**	0.7750	0.6159	0.6152	0.9433
5	Condition 2	Condition 1	RMSE	**0.8600**	1.5764	1.3185	2.8598	4.1400
	No.91, No.100	No.2	MAPE	**0.7339**	1.2629	1.1345	2.1817	2.9793
6	Condition 4	Condition 3	RMSE	**0.1956**	0.4172	0.3954	1.0123	1.7137
	No.93, No.113, No.120	No.85	MAPE	**0.1290**	0.3615	0.2528	0.8297	0.8297

testing sample is No. 2 battery. All batteries are from condition 1. Cases 3 and 4 are VC fast charging conditions. In case 3, the training samples are No. 85, No. 107, and No.115 batteries and the testing sample is No. 119 battery. All batteries are from Condition 3. Cases 5 and 6 are cross fast charging conditions, where the charging conditions of the training and test samples are different. In case 5, the training samples are No. 91 and No. 100 from Condition 2, and the testing sample is No. 2 battery from Condition 1. In case 6, the training samples are No. 93, No. 113, and No. 120 from Condition 4, and the testing sample is No. 85 battery from Condition 3. All the fast charging methods of five Conditions can be referred to Fig. 1.

4.3.1. CC fast charging conditions

Fig. 6 shows the predicted capacity and error results of cases 1 and 2, where CC fast charging conditions are used. The capacity prediction RMSEs of cases 1 and 2 are 0.3350% and 0.2820%, respectively. The good results demonstrate that the proposed method can be well used for CC fast charging conditions.

4.3.2. VC fast charging conditions

Fig. 7 presents the results of cases 3 and 4 in VC fast charging conditions. In case 3, the capacity degradation curves between the training samples (No.85, No.107, and No.115) and the testing cell (No.119) are considerably different. As shown in Fig. 1(d), the biggest difference between training and testing battery life is more than 1000 cycles. In this case, the prediction RMSE and MAPE with $V_{80\%}$ + Cn as the model feature are 0.3972% and 0.3190%, which are significantly lower than those of the other four features. Similar experimental results occur in case 4. The comparison results reveal that the proposed method is feasible in VC fast charging conditions.

4.3.3. Cross fast charging conditions

Fig. 8 shows the model performance of cases 5 and 6 under cross fast charging conditions. In case 5, the prediction RMSE and MAPE are 0.8600% and 0.7339%, which are the lowest compared to the model performance of the other four features. Although they are slightly larger than those in cases 1–4, it is reasonable because the

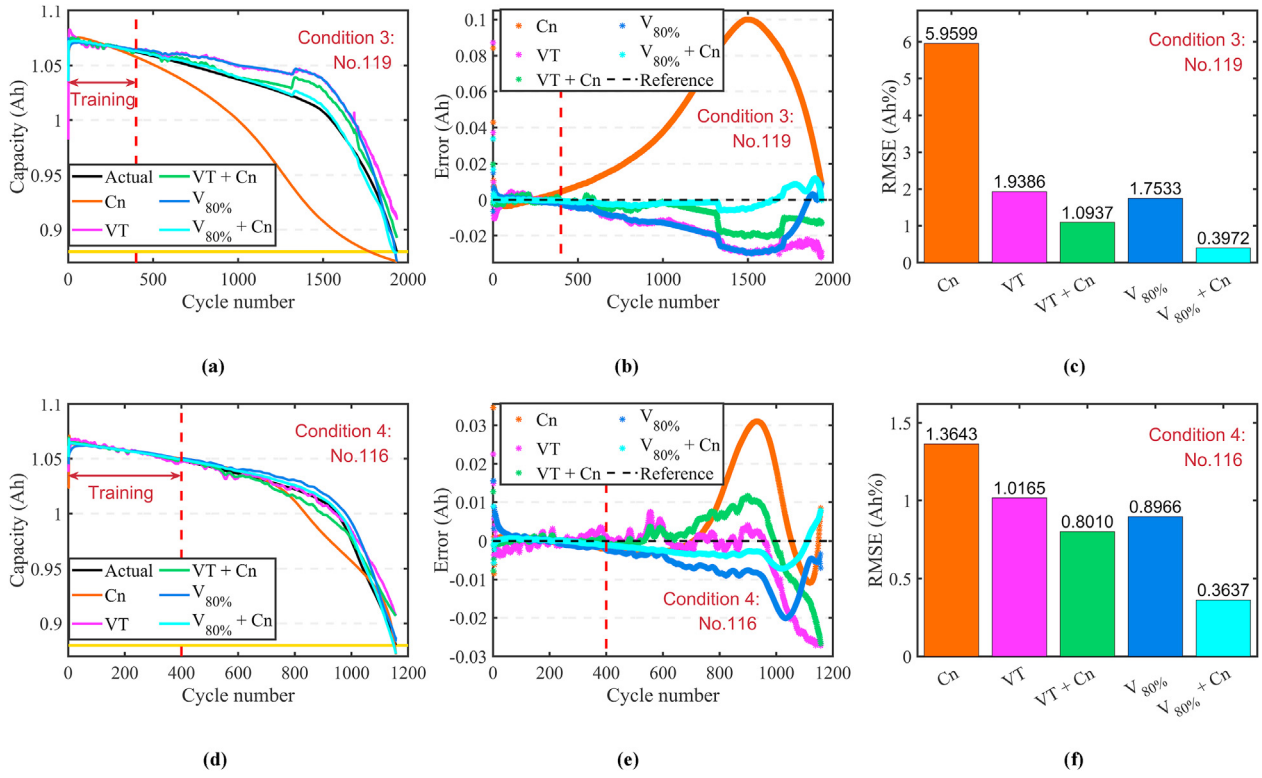

Fig. 7. Capacity prediction performance for VC fast charging conditions. **(a)**, **(b)** and **(c):** Case 3; **(d)**, **(e)** and **(f):** Case 4.

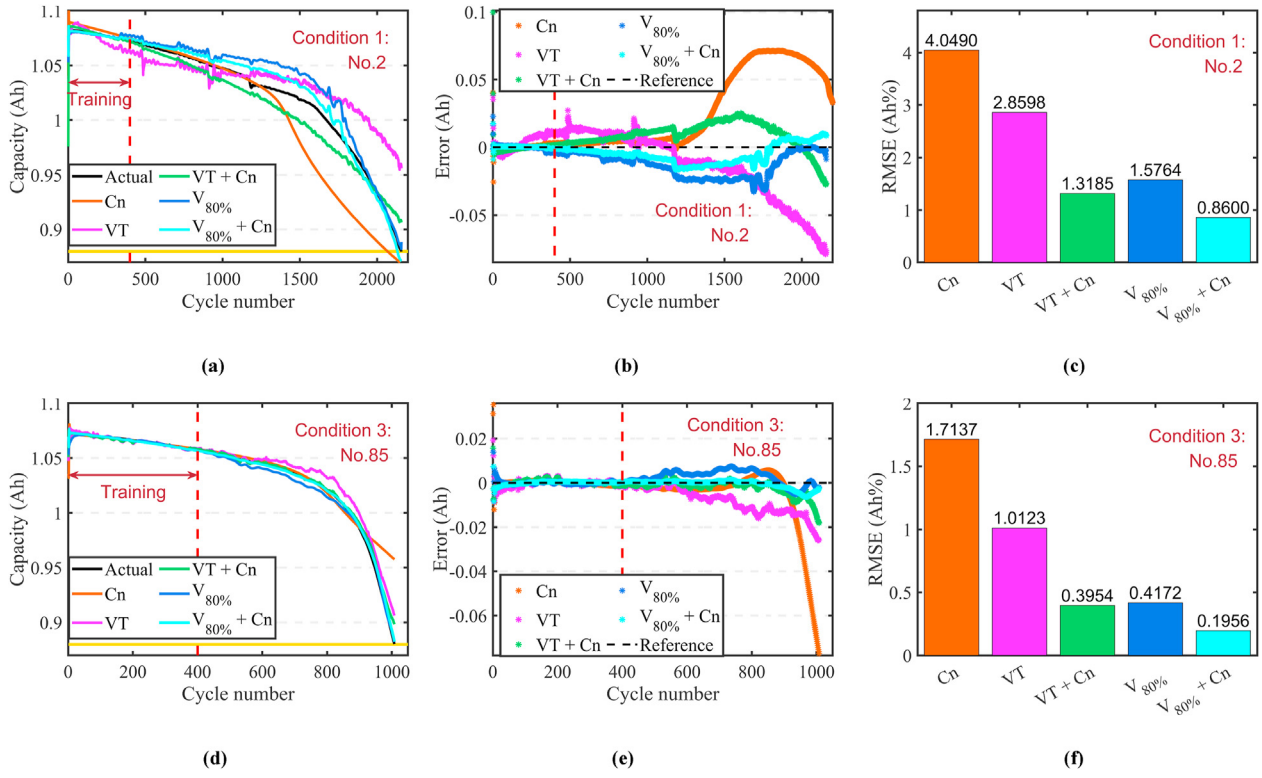

Fig. 8. Capacity prediction performance of cross fast charging conditions. **(a)**, **(b)** and **(c):** Case 5; **(d)**, **(e)** and **(f):** Case 6.

charging conditions of the training and testing samples are different. In case 6, the prediction RMSE and MAPE are 0.1956% and 0.1290%. It is an acceptable experimental result since all evaluation criteria are less than 1%.

Table 5
Numerical results of model complexity.

Stages	Operations (s)	Case No.					
		1	2	3	4	5	6
Offline	Training	112.643	95.741	88.522	90.489	98.301	89.769
Online	Finetuning	1.088	1.126	0.977	0.989	1.046	1.035
	Prediction	0.011	0.011	0.011	0.011	0.011	0.011

In summary, the proposed method has high adaptability. As cases 1–4 show, it can achieve good capacity prediction performance for the same batch of batteries under the same charging conditions. The experimental results in cases 5–6 also demonstrate that the proposed method is adaptive and can effectively deal with the threat of capacity prediction caused by the cell-to-cell differences.

4.4. Model complexity evaluation

All experiments are performed on a Lenovo ThinkCentre PC520C computer with Intel Xeon W-2175 (2.50 GHz) CPU, 128-GB RAM, Nvidia Quadro RTX-4000 graphics card, and Windows 10 (64-bit) system. Data processing and prediction modeling are completed on MATLAB 2020b. The computational time of six cases is summarized in Table 5. The experimental results are averaged from five runs. The offline training takes less than 2 min. The online finetuning time is near 1 s, while the prediction time is 0.011 s. Therefore, the online application of the proposed method in a practical BMS is feasible.

5. Conclusion

This paper proposes a new LSTM–FC–based transfer learning model for adaptive online prediction of battery capacity under fast charging. First, a novel feature $V_{80\%}$ + Cn is constructed by integrating the 80% SOC charging voltage and the cycle number through SW technology. It has high practicability, and its effectiveness has been verified by Pearson correlation analysis. Then, a cross-validation method with both high- and low-similarity tasks is performed to provide the optimal hyperparameters for highly adaptable modeling. Next, the existing battery data are used to train the LSTM-FC network offline. The well-trained model is sent to the online application to reduce the computational burden. Finally, the early data from the new battery is used to finetune the FC layer for online capacity prediction. To verify the superiority of the proposed feature, four other features, including $V_{80\%}$, Cn, VT, and VT + Cn, have been added for comparison. The experimental results show that with the $V_{80\%}$ + Cn feature as the model input, the prediction RMSE and MAPE are the lowest. In addition, six experiments with CC, VC, and cross fast charging conditions have been carried out. The proposed method can achieve satisfactory modeling performance in all situations, which greatly proves its high adaptability.

The proposed method only considers the fast charging conditions and manufacturing variability of a single cell. In future research, we will focus on the following two aspects:

1) More factors that lead to different degradation behaviors of LIBs, including temperature, depth of discharge, and mechanical stress [1,7], will be incorporated into the model.
2) The highly adaptable solution will be extended to the battery pack system to solve the inconsistency and nonlinear aging modeling problems between multiple cells.

Credit author statement

Zhang Chen: Conceptualization, Investigation, Methodology, Data curation, Software, Validation, Roles/Writing - original draft, Writing – review & editing; **Wenjing Shen**: Formal analysis, Investigation, Project administration; Resources, Funding acquisition, Supervision, Validation, Writing – review & editing; **Liqun Chen**: Methodology, Formal analysis, Investigation, Validation, Writing – review & editing; **Shuqiang Wang**: Formal analysis, Validation, Writing – review & editing.

Declaration of competing interest

The authors declare that they have no known competing financial interests or personal relationships that could have appeared to influence the work reported in this paper.

Acknowledgments

This work was supported in part by the National Natural Science Foundation of China under Grant 51906160, in part by the Guangdong Basic and Applied Basic Research Foundation under Grant 2018A030313747, in part by the Natural Science Foundation of Top Talent of SZTU under Grant 1814309011180003, and in part by the school-enterprise cooperation project of SZTU under Grant 20213108010001.

Appendix A. Supplementary data

Supplementary data to this article can be found online at https://doi.org/10.1016/j.energy.2022.123537.

References

[1] Hu X, Xu L, Lin X, Pecht M. Battery lifetime prognostics. Joule 2020;4:310–46. https://doi.org/10.1016/j.joule.2019.11.018.
[2] Sun T, Xu B, Cui Y, Feng X, Han X, Zheng Y. A sequential capacity estimation for the lithium-ion batteries combining incremental capacity curve and discrete arrhenius fading model. J Power Sources 2021;484:229248. https://doi.org/10.1016/j.jpowsour.2020.229248.
[3] Zhang X, Wang Y, Liu C, Chen Z. A novel approach of battery pack state of health estimation using artificial intelligence optimization algorithm. J Power Sources 2018;376:191–9. https://doi.org/10.1016/j.jpowsour.2017.11.068.
[4] Hu X, Che Y, Lin X, Onori S. Battery health prediction using fusion-based feature selection and machine learning. IEEE Trans. Transport. Electrific. 2021;7:382–98. https://doi.org/10.1109/tte.2020.3017090.
[5] Xiong R, Pan Y, Shen W, Li H, Sun F. Lithium-ion battery aging mechanisms and diagnosis method for automotive applications: recent advances and perspectives. Renew Sustain Energy Rev 2020;131:110048. https://doi.org/10.1016/j.rser.2020.110048.
[6] Cannarella J, Arnold CB. Ion transport restriction in mechanically strained separator membranes. J Power Sources 2013;226:149–55. https://doi.org/10.1016/j.jpowsour.2012.10.093.
[7] Weng A, Mohtat P, Attia PM, Sulzer V, Lee S, Less G, Stefanopoulou A. Predicting the impact of formation protocols on battery lifetime immediately after manufacturing. Joule 2021;5:2971–92. https://doi.org/10.1016/j.joule.2021.09.015.
[8] Birkl CR, Roberts MR, McTurk E, Bruce PG, Howey DA. Degradation diagnostics for lithium ion cells. J Power Sources 2017;341:373–86. https://doi.org/10.1016/j.jpowsour.2016.12.011.
[9] Ng M-F, Zhao J, Yan Q, Conduit GJ, Seh ZW. Predicting the state of charge and health of batteries using data-driven machine learning. Nat. Mach. Intell. 2020;2:161–70. https://doi.org/10.1038/s42256-020-0156-7.
[10] Nejad S, Gladwin DT, Stone DA. A systematic review of lumped-parameter equivalent circuit models for real-time estimation of lithium-ion battery states. J Power Sources 2016;316:183–96. https://doi.org/10.1016/j.jpowsour.2016.03.042.
[11] Johnson VH. Battery performance models in advisor. J Power Sources 2002;110:321–9. https://doi.org/10.1016/S0378-7753(02)00194-5.
[12] Lai X, Yi W, Cui Y, Qin C, Han X, Sun T, Zhou L, Zheng Y. Capacity estimation of lithium-ion cells by combining model-based and data-driven methods based on a sequential extended kalman filter. Energy 2021;216:119233. https://doi.org/10.1016/j.energy.2020.119233.
[13] Hu X, Li S, Peng H. A comparative study of equivalent circuit models for Li-ion

batteries. J Power Sources 2012;198:359–67. https://doi.org/10.1016/j.jpowsour.2011.10.013.
[14] Hu X, Yuan H, Zou C, Li Z, Zhang L. Co-estimation of state of charge and state of health for lithium-ion batteries based on fractional-order calculus. IEEE Trans Veh Technol 2018;67:10319–29. https://doi.org/10.1109/tvt.2018.2865664.
[15] Hu X, Jiang H, Feng F, Liu B. An enhanced multi-state estimation hierarchy for advanced lithium-ion battery management. Appl Energy 2020;257:114019. https://doi.org/10.1016/j.apenergy.2019.114019.
[16] Li Y, Liu K, Foley AM, Zülke A, Berecibar M, Nanini-Maury E, Van Mierlo J, Hoster HE. Data-driven health estimation and lifetime prediction of lithium-ion batteries: a review. Renew Sustain Energy Rev 2019;113:109254. https://doi.org/10.1016/j.rser.2019.109254.
[17] Klass V, Behm M, Lindbergh G. A support vector machine-based state-of-health estimation method for lithium-ion batteries under electric vehicle operation. J Power Sources 2014;270:262–72. https://doi.org/10.1016/j.jpowsour.2014.07.116.
[18] Patil MA, Tagade P, Hariharan KS, Kolake SM, Song T, Yeo T, Doo S. A novel multistage support vector machine based approach for Li ion battery remaining useful life estimation. Appl Energy 2015;159:285–97. https://doi.org/10.1016/j.apenergy.2015.08.119.
[19] Li X, Yuan C, Wang Z. State of health estimation for Li-ion battery via partial incremental capacity analysis based on support vector regression. Energy 2020;203:117852. https://doi.org/10.1016/j.energy.2020.117852.
[20] Wang D, Kong J-Z, Zhao Y, Tsui K-L. Piecewise model based intelligent prognostics for state of health prediction of rechargeable batteries with capacity regeneration phenomena. Measurement 2019;147:106836. https://doi.org/10.1016/j.measurement.2019.07.064.
[21] Wang D, Miao Q, Pecht M. Prognostics of lithium-ion batteries based on relevance vectors and a conditional three-parameter capacity degradation model. J Power Sources 2013;239:253–64. https://doi.org/10.1016/j.jpowsour.2013.03.129.
[22] Richardson RR, Osborne MA, Howey DA. Gaussian process regression for forecasting battery state of health. J Power Sources 2017;357:209–19. https://doi.org/10.1016/j.jpowsour.2017.05.004.
[23] Kong J-z, Yang F, Zhang X, Pan E, Peng Z, Wang D. Voltage-temperature health feature extraction to improve prognostics and health management of lithium-ion batteries. Energy 2021;223:120114. https://doi.org/10.1016/j.energy.2021.120114.
[24] Dai H, Zhao G, Lin M, Wu J, Zheng G. A novel estimation method for the state of health of lithium-ion battery using prior knowledge-based neural network and Markov chain. IEEE Trans Ind Electron 2019;66:7706–16. https://doi.org/10.1109/tie.2018.2880703.
[25] Ji Y, Chen Z, Shen Y, Yang K, Wang Y, Cui J. An rul prediction approach for lithium-ion battery based on sade-mesn. Appl Soft Comput 2021;104:107195. https://doi.org/10.1016/j.asoc.2021.107195.
[26] Hochreiter S, Schmidhuber J. Long short-term memory. Neural Comput 1997;9:1735–80. https://doi.org/10.1162/neco.1997.9.8.1735.
[27] You G-W, Park S, Oh D. Diagnosis of electric vehicle batteries using recurrent neural networks. IEEE Trans Ind Electron 2017;64:4885–93. https://doi.org/10.1109/tie.2017.2674593.
[28] Li W, Sengupta N, Dechent P, Howey D, Annaswamy A, Sauer DU. Online capacity estimation of lithium-ion batteries with deep long short-term memory networks. J Power Sources 2021;482:228863. https://doi.org/10.1016/j.jpowsour.2020.228863.
[29] Li W, Sengupta N, Dechent P, Howey D, Annaswamy A, Sauer DU. One-shot battery degradation trajectory prediction with deep learning. J Power Sources 2021;506:230024. https://doi.org/10.1016/j.jpowsour.2021.230024.
[30] Zhang Y, Xiong R, He H, Pecht MG. Long short-term memory recurrent neural network for remaining useful life prediction of lithium-ion batteries. IEEE Trans Veh Technol 2018;67:5695–705. https://doi.org/10.1109/tvt.2018.2805189.
[31] Cheng G, Wang X, He Y. Remaining useful life and state of health prediction for lithium batteries based on empirical mode decomposition and a long and short memory neural network. Energy 2021;232:121022. https://doi.org/10.1016/j.energy.2021.121022.
[32] Liu K, Shang Y, Ouyang Q, Widanage WD. A data-driven approach with uncertainty quantification for predicting future capacities and remaining useful life of lithium-ion battery. IEEE Trans Ind Electron 2021;68:3170–80. https://doi.org/10.1109/tie.2020.2973876.
[33] Che Y, Deng Z, Lin X, Hu L, Hu X. Predictive battery health management with transfer learning and online model correction. IEEE Trans Veh Technol 2021;70:1269–77. https://doi.org/10.1109/tvt.2021.3055811.
[34] Tan Y, Zhao G. Transfer learning with long short-term memory network for state-of-health prediction of lithium-ion batteries. IEEE Trans Ind Electron 2020;67:8723–31. https://doi.org/10.1109/tie.2019.2946551.
[35] Deng Z, Lin X, Cai J, Hu X. Battery health estimation with degradation pattern recognition and transfer learning. J Power Sources 2022;525:231027. https://doi.org/10.1016/j.jpowsour.2022.231027.
[36] Tian J, Xiong R, Shen W, Lu J, Yang X-G. Deep neural network battery charging curve prediction using 30 points collected in 10 min. Joule 2021;5:1521–34. https://doi.org/10.1016/j.joule.2021.05.012.
[37] Xu T, Peng Z, Wu L. A novel data-driven method for predicting the circulating capacity of lithium-ion battery under random variable current. Energy 2021;218. https://doi.org/10.1016/j.energy.2020.119530. 119530.
[38] Tan X, Zhan D, Lyu P, Rao J, Fan Y. Online state-of-health estimation of lithium-ion battery based on dynamic parameter identification at multi timescale and support vector regression. J Power Sources 2021;484:229233. https://doi.org/10.1016/j.jpowsour.2020.229233.
[39] Severson KA, Attia PM, Jin N, Perkins N, Jiang B, Yang Z, Chen MH, Aykol M, Herring PK, Fraggedakis D, Bazant MZ, Harris SJ, Chueh WC, Braatz RD. Data-driven prediction of battery cycle life before capacity degradation. Nat Energy 2019;4:383–91. https://doi.org/10.1038/s41560-019-0356-8.
[40] Wang Z, Zeng S, Guo J, Qin T. State of health estimation of lithium-ion batteries based on the constant voltage charging curve. Energy 2019;167:661–9. https://doi.org/10.1016/j.energy.2018.11.008.
[41] Fei Z, Yang F, Tsui K-L, Li L, Zhang Z. Early prediction of battery lifetime via a machine learning based framework. Energy 2021;225:120205. https://doi.org/10.1016/j.energy.2021.120205.
[42] Bian X, Liu L, Yan J. A model for state-of-health estimation of lithium ion batteries based on charging profiles. Energy 2019;177:57–65. https://doi.org/10.1016/j.energy.2019.04.070.
[43] Li X, Yuan C, Li X, Wang Z. State of health estimation for Li-ion battery using incremental capacity analysis and Gaussian process regression. Energy 2020;190:116467. https://doi.org/10.1016/j.energy.2019.116467.
[44] Lui YH, Li M, Downey A, Shen S, Nemani VP, Ye H, VanElzen C, Jain G, Hu S, Laflamme S, Hu C. Physics-based prognostics of implantable-grade lithium-ion battery for remaining useful life prediction. J Power Sources 2021;485:229327. https://doi.org/10.1016/j.jpowsour.2020.229327.
[45] Hosen MS, Jaguemont J, Van Mierlo J, Berecibar M. Battery lifetime prediction and performance assessment of different modeling approaches. iScience 2021;24:102060. https://doi.org/10.1016/j.isci.2021.102060.
[46] Baumhöfer T, Brühl M, Rothgang S, Sauer DU. Production caused variation in capacity aging trend and correlation to initial cell performance. J Power Sources 2014;247:332–8. https://doi.org/10.1016/j.jpowsour.2013.08.108.
[47] Lipu MSH, Hannan MA, Hussain A, Hoque MM, Ker PJ, Saad MHM, Ayob A. A review of state of health and remaining useful life estimation methods for lithium-ion battery in electric vehicles: challenges and recommendations. J Clean Prod 2018;205:115–33. https://doi.org/10.1016/j.jclepro.2018.09.065.
[48] Wang B-C, Li H-X. A sliding window based dynamic spatiotemporal modeling for distributed parameter systems with time-dependent boundary conditions. IEEE Trans Ind Inf 2019;15:2044–53. https://doi.org/10.1109/tii.2018.2859444.
[49] Kingma DP, Ba JL. Adam: a method for stochastic optimization. *arXiv: 1412.6980 [cs.LG]*, https://arxiv.org/abs/1412.6980; 2015.
[50] Srivastava N, Hinton G, Krizhevsky A, Sutskever I, Salakhutdinov R. Dropout: a simple way to prevent neural networks from overfitting. J Mach Learn Res 2014;15:1929–58. https://dl.acm.org/doi/10.5555/2627435.2670313.
[51] Pan SJ, Yang Q. A survey on transfer learning. IEEE Trans Knowl Data Eng 2010;22:1345–59. https://doi.org/10.1109/TKDE.2009.191.